



Contents lists available at ScienceDirect

Spectrochimica Acta Part B: Atomic Spectroscopy

journal homepage: www.elsevier.com/locate/sab

Signal enhancement with double-pulse LIBS on biological samples and better discrimination of tissues through machine learning algorithms

Elena Ramela Ciobotea^a, Cristian Sarpe^a, Bastian Zielinski^{a,b}, Hendrike Braun^a, Arne Senftleben^a, Soumi Dutta^c, Georg Mayer^c, Camilo Florian^{a,b}, Thomas Baumert^{a,*}^a University of Kassel, Institute of Physics, Heinrich-Plett-Str. 40, 34132 Kassel, Germany^b University of Kassel, Institute of Materials Engineering, Moenchebergstr. 7, 34125 Kassel, Germany^c University of Kassel, Institute of Biology, Heinrich-Plett-Str. 40, 34132 Kassel, Germany

ARTICLE INFO

Keywords:

fs-DP-LIBS

ML algorithms

Signal enhancement

Thin biological samples

ABSTRACT

Laser-induced breakdown spectroscopy (LIBS) is a widely used technique in the field of spectroscopy, enabling the determination of the chemical composition of a variety of samples using typically single laser pulses. This paper presents the successful integration of femtosecond LIBS using double pulses that combined with machine learning algorithms enhanced the discrimination between two animal tissue types (liver and muscle) through the detection of atomic and molecular emissions. The double-pulse configuration was optimized on liver tissue, and the results demonstrated that at 1100 ps pulse delay, the signal was the highest overall for all identified lines, with a fivefold increase compared to single-pulse configuration at comparable energies. By employing femtosecond double-pulse LIBS, it is possible to achieve enhanced signal quality with a better signal-to-noise ratio. Both algorithms used here (Artificial Neural Network and Random Forest) consequently demonstrate superior performance in tissue type prediction when double pulses are employed, as compared to single pulses. The combination of femtosecond double-pulse LIBS with machine learning algorithms has the potential to be an effective technique for thin biological samples (for example biopsy sections), with minimal ablation.

1. Introduction

Laser-induced breakdown spectroscopy (LIBS) has been a popular analytical technique for decades, providing fast and accurate results for studying the elemental composition of various materials. This method is based on the information extracted from plasma generated by the laser-matter interaction. The spectral lines observed at certain wavelengths correspond to specific elements in the sample. This technique's simplicity, high spatial resolution and real-time assessment have contributed to its widespread adoption across various fields [1–6].

The use of high-energy pulsed lasers is the standard approach for the implementation of LIBS. These lasers typically operate in the nanosecond (ns) range, offering the advantages of cost-effectiveness, durability, and versatility. Using femtosecond-LIBS (fs-LIBS) can offer advantages like efficient ablation, lower continuous emission or better discrimination of the molecular bands in complex samples [7–10]. However, the plasma generated by a fs laser pulse generally has a smaller volume and lower temperature, which results in lower signal

intensity and places a higher demand on detection [11]. The accuracy of the results produced by both laser types (ns and fs) depends on the application and material in question, as both have been employed in enhancing spectral intensity through various methods [12–16].

The double-pulse LIBS (DP-LIBS) approach represents one of the most frequently used methods in a wide range of samples, configurations or combinations of ns and fs lasers to achieve higher spectral intensities [17–24]. The principle of DP-LIBS is based on the generation of plasma by a first laser pulse, followed by additional energy deposition into this plasma with a second laser pulse, which is applied after a specific time interval (referred to as the inner pulse delay). This results in a higher energy content within the plasma and, subsequently, enhanced optical emission.

The versatility of LIBS as a characterization technique lies in different factors; it does not require extensive sample preparation such as fixation and specific labeling or staining of tissue, allows for rapid data acquisition, is operational in ambient conditions, and is capable of identifying a wide range of elements, which makes it a suitable method

* Corresponding author.

E-mail address: tbaumert@uni-kassel.de (T. Baumert).<https://doi.org/10.1016/j.sab.2024.107063>

Received 21 August 2024; Received in revised form 28 October 2024; Accepted 30 October 2024

Available online 2 November 2024

0584-8547/© 2024 The Authors. Published by Elsevier B.V. This is an open access article under the CC BY license (<http://creativecommons.org/licenses/by/4.0/>).

for analyzing biological samples. In the field of medical research, LIBS has been adopted as a tool for multi-element analysis [14,25], elemental imaging [26–28], tissue classification [29], bacterial detection [30] and the characterization of certain specific malignant cells [25,31]. This resulted in the generation of a large quantity of data, necessitating the development of new chemometric tools to facilitate the visualization and characterization of LIBS spectra [14,32–35]. The integration of advanced spectroscopic techniques, such as DP-LIBS, with sophisticated chemometrics tools, like Machine Learning (ML) algorithms, is a relatively new approach, mainly used in the analysis of soil samples, to check for traces of metals and estimate their limit of detection [36]. Our previous study demonstrated the advantages of using single-pulse LIBS (SP-LIBS) in combination with ML algorithms on thin pathological human samples to differentiate cancerous tissue [35].

This paper successfully integrates the fs-DP-LIBS with ML algorithms, enabling the discrimination between two tissue types through the identification of atomic and molecular emissions. In the initial section, we provide an overview of the technical aspects of the laser system, a detailed examination of the samples, the acquisition of spectral data, and the employed methodologies for data processing. The following section presents the signal enhancement that can be attained through DP-LIBS on animal tissue, as well as the resulting enhancement of the discrimination that can be achieved between the two tissues when using the SP-LIBS and DP-LIBS techniques. Furthermore, the SNR for the most pronounced lines is discussed.

2. Material and methods

2.1. Sample preparation

In this study, fresh bovine tissue (liver and muscle) was collected from a local butcher and transferred to the laboratory for cryosectioning. This method was selected due to its rapidity, simplicity, and suitability, allowing the tissue to freeze rapidly and preventing the formation of crystals.

Small samples ($5 \times 5 \times 5 \text{ mm}^3$) were prepared for cryostat sectioning using the standard procedure which involved embedding in an optimal cutting temperature compound (OCT; Tissue-Tek® O.C.T. Compound, Sakura Finetek USA, Inc.) in a cryomold, followed by snap freezing the cryomold in liquid nitrogen. Subsequently, the frozen tissue block was transferred to the cryostat chamber, and equilibrated for at least 20 min to the preset chamber temperature ($-23 \text{ }^\circ\text{C}$ for bovine muscle and $-25 \text{ }^\circ\text{C}$ for bovine liver) before cutting into sections. A series of cryogenic sections of $30 \text{ }\mu\text{m}$ were obtained for each tissue type (liver and muscle) and mounted on a high purity quartz microscope slide (Plano GmbH). This substrate has been identified as a suitable candidate for spectral

analysis [35], due to the absence of additives (chemical elements other than silicon and oxygen) that might potentially interfere with the detection of the intended biological signal. Furthermore, the pure substrate (just Si line) exhibits no spectral overlap with the sample spectrum, which is essential for the accurate interpretation of the biological signal.

Fig. 1A illustrates the sample preparation steps. Fig. 1B and C show actual examples of the millimeter sized sections on the substrate with marked regions of interest (left part) and microscopic images of the tissue after LIBS ablation (right part). In the ablation process it was ensured that only unaltered tissue was selected by avoiding areas near the border with the OCT and holes in the tissue. In most cases, a 10×10 matrix of laser ablation spots was generated at the selected tissue location. However, in some instances, the matrix size was adjusted to accommodate the available area, due to the presence of ruptures (micro-holes) in the tissue, particularly in muscle tissue. Each point in the matrix generates an individual LIBS spectrum.

2.2. Experimental setup

The experimental setup employed in this study was analogous to that used in previous studies [35] with the addition of a Mach–Zehnder interferometer to produce double pulses with variable delay that is depicted in Fig. 2. A bandwidth-limited pulse (30 fs duration at 785 nm central wavelength) was directed towards a pulse shaper to compensate for the dispersion at the interaction area, and subsequently to the interferometer, resulting in the generation of a pair of pulses. These pulses were delayed by the delay lines DL1 and DL2 and recombined prior to entering the focusing objective (Mitutoyo M Plan Apo 10 \times , NA = 0.28). DL1 (with a total travel range of 500 ps) was employed for fine adjustments in determining the time zero between the pulses, whereas DL2, due to its greater travel range of 5 ns (-2 ns and $+3 \text{ ns}$ from time zero), was used to vary the delay between the pulses. The position of the sample was continuously monitored by a camera and adjusted using an XYZ translation stage. Spatial overlap of the pair of pulses was ensured for each new delay step by first observing the creation of damage in a glass microscope slide with the monitoring camera (see Fig. 2) and adjusting one beam line accordingly. The ablation of biological samples was done with peak intensities of $2.4 \times 10^{15} \text{ W/cm}^2$ for the case of $14 \text{ }\mu\text{J}$ pulse energy and $3.5 \times 10^{15} \text{ W/cm}^2$ for $20 \text{ }\mu\text{J}$ pulse energy with a measured gaussian beam radius of $3.5 \text{ }\mu\text{m}$ at $1/e^2$. The emitted light from the created plasma is collected by a pair of fused silica lenses (positioned at 45° close to the microscope objective) and directed to the spectrometer (L.O.T. Oriel Multispec MS125) and a gated Intensified CCD camera (Roper Scientific PIMAX ICCD), recording spectra with 1024 pixels. Each laser pulse or pair of pulses ablated a single spot on the

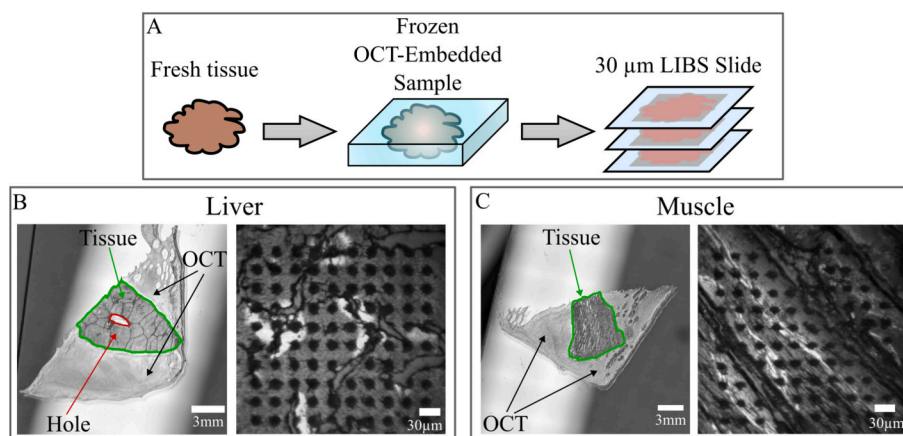


Fig. 1. Sample preparation in A and tissue comparison for the cryosection of the liver in B-left and muscle in C-left. The right picture in B and C presents an optical microscopic image of the 10×10 matrix after LIBS ablation. OCT represents the Optimal Cutting Temperature compound in which the tissue is embedded.

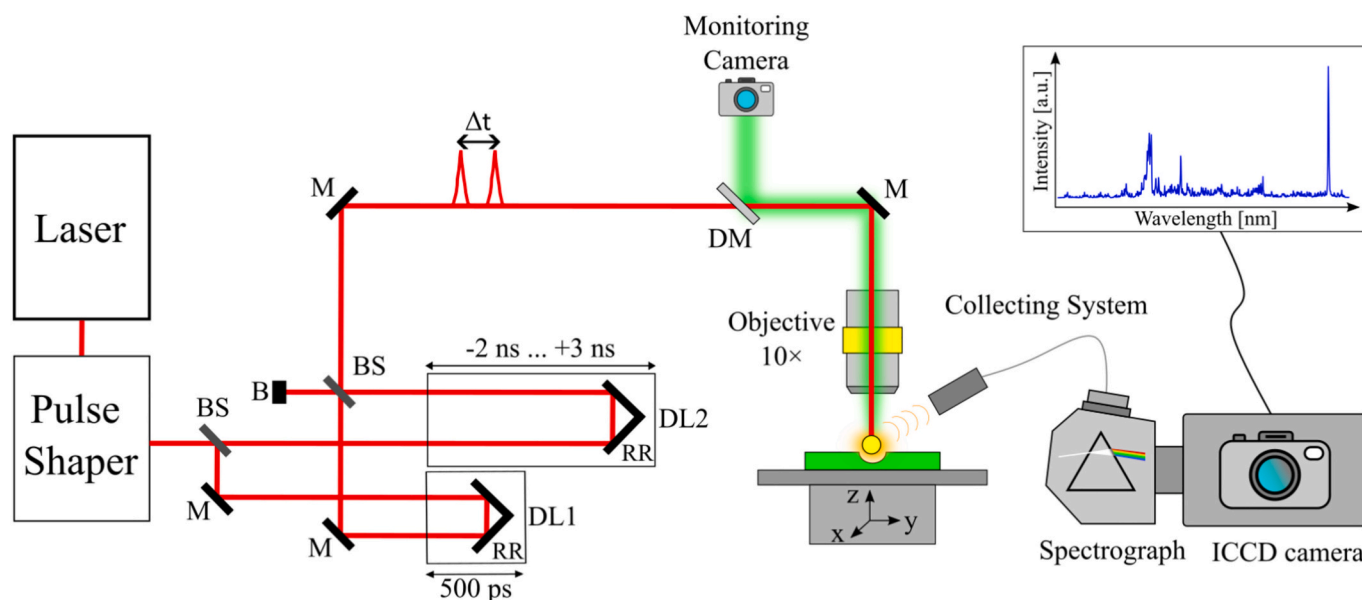


Fig. 2. Schematic representation of the experimental setup of DP-LIBS and spectra recording. BS: Beam Splitter, M: Mirror, B: Blocker, RR: Retro Reflector, DM: Dichroic Mirror, DL1 and DL2: Delay Line 1 and 2, Δt : time delay.

sample, resulting in the generation of one spectrum, which was recorded for a gate time of 500 ns after the continuum emission from bremsstrahlung and radiative recombination.

2.3. Data processing and machine learning

Once all spectra had been gathered, they were processed further. Each data set was collected on the same day under identical conditions, thus eliminating the potential influence of external factors [35]. The initial step was to assign a label to each spectrum using a self-developed program in LabView, followed by a series of data processing steps in the Orange data mining software [37]. All acquired spectra were imported into Orange, grouped according to distinct categories (tissue type and pulse type), and then subjected to two outlier removals. The first removal was conducted via a local outlier factor algorithm with 5 % contamination for 25 neighbors, with the purpose of eliminating anomalous spectra. The second removal was necessary for the samples that contained cracks to rule out ablation on the substrate, rather than the tissue itself. These spectra had to be excluded from the data set. This is achieved by applying a suitable outlier threshold for a specific pixel of the spectrum belonging to the Si line, which then results in the removal of that entire spectrum. The percentage of removed spectra from the entire data set was between 4 % and 6 %.

From this point onwards, the data were processed in a different manner for the purposes of displaying the signal enhancement in Fig. 3 and for the results obtained through the application of machine learning in Fig. 4. In the first case, the initial 10 pixels and the final 10 pixels of the acquired signal were removed (due to no light reaching the corners of the CCD sensor) and a linear baseline subtraction was performed automatically in the software Orange for each single spectrum by using the existing widget 'Preprocess Spectra'. The spectra were averaged for each delay, and a selection of them is presented in Fig. 3.

In the second case, three adjacent spectra were averaged, as the laser spots were smaller than the corresponding tissue cell and the heterogeneity of the tissue necessitated such an approach. The initial and final 10 pixels were removed and the data underwent baseline subtraction as indicated before, and additional vector normalization. The final spectra were suitable for use with machine learning algorithms, including Artificial Neural Networks (ANN) and Random Forest (RF), using a 'test and score' classification with tenfold cross-validation as a sampling

method. ANN was trained with a network of 512 neurons, while RF was configured with 250 trees. The results from the performance of the algorithms are presented in Fig. 4.

3. Results and discussion

3.1. Signal enhancement with double pulse LIBS

To measure the enhancement of the LIBS signal with double pulses, the cryosectioned liver tissue was initially ablated with a 20 μJ single laser pulse (one arm of the interferometer blocked). The resulting spectra from each ablation spot were recorded and subsequently processed. For acquiring the DP-LIBS, the laser energy was adjusted to 10 μJ for each of the two pulses, so that the sum will be identical to SP energy. A wide range of successive inner pulse delays was scanned, excluding time zero due to interference effects, and extending to 3320 ps (the maximum range of DL2 for the current setup). All spectra were pre-processed in Orange, as described in the previous section, leaving 200–350 suitable spectra for each inner delay, which are presented in Fig. 3 A. The spectra are color-coded to show the highest intensity in black or dark red and lower intensities in green, light blue and dark blue. Additionally, the atomic lines (Mg I, Ca II, Ca I, Na I) and molecular fragments (C–N, C–H, C–C) were identified [38,39] and labelled, with arrows pointing at the top of the peak/bands for the SP spectrum. Other spectral signatures were considered to be relatively weak and therefore not suitable for the enhancement analysis.

A preliminary examination of the inner delay parameter at 200 ps indicates the presence of a signal enhancement compared to SP measurements and exhibits new lines such as Ca II and Mg I. At an inner delay of 1100 ps, the signal reaches a fivefold increase compared to the SP signal for the Ca II line, fourfold for Ca I, twofold for Na, and slightly above threefold for the C–N, C–H, C–C bands. The signal decreases at longer delays.

Fig. 3 B provides a more detailed view of all identified atomic lines (left part) and molecular bands (right part), with each point representing the respective enhancement factor for each inner pulse delay measurement. The enhancement factor for each peak/band was calculated by dividing the area under the curve for that peak/band by the area under the curve for the signal measured with SP. A rapid increase of signal is observed in all the graphs (< 200 ps), with the

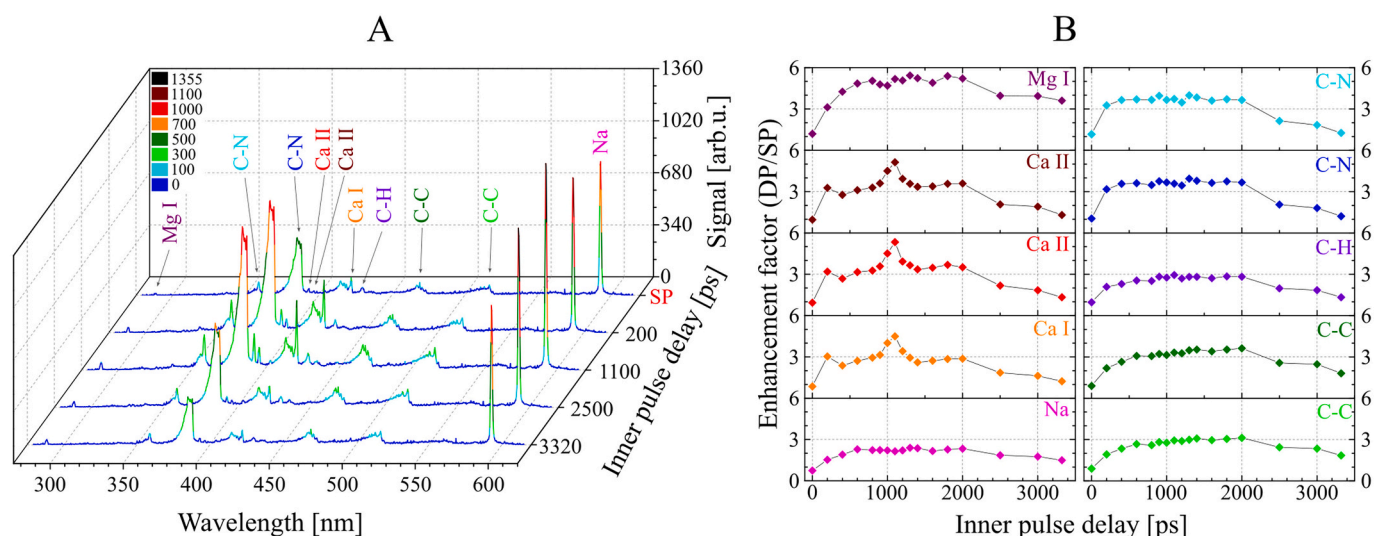


Fig. 3. A - Emission intensities of liver tissue as a function of inner pulse delay. The back-most spectrum (marked SP in red on the inner pulse delay scale) is from SP-LIBS at comparable energy with DP-LIBS. The intensities were color-coded from low value (blue, green) to high value (red, black). B - Enhancement factor (DP-signal/SP-signal) as a function of inner pulse delay for all identified atomic lines (left part) and molecular bands (right part), based on the area under the respective signal. (For interpretation of the references to color in this figure legend, the reader is referred to the web version of this article.)

presence of a plateau starting at 200 ps (for all Ca lines) and 600 ps for all the others, until 2000 ps. In contrast, a decrease in signal is observed for longer inner pulse delays. The plateau presents a constant enhancement factor of approximately threefold for most lines, except for the Mg I line, where the plateau is slightly under sixfold enhancement.

In our previous experiment [17], we demonstrated that in both aluminum and titanium samples the DP-LIBS signal begins to rise at an inner delay of between 1 and 10 ps, subsequently increasing continuously between 10 and 100 ps, after which it reaches a constant signal at the end of this region. Following a 100 ps inner delay, there was a further increase in the signal, although with a smaller slope, reaching a maximum enhancement at an inner delay of 800 ps, with a subsequent decrease in signal at longer delays. In other experiments [40], it has been shown that the spectral intensity (meaning both peak height and peak area) of the DP-LIBS depends on the plasma plume, which for materials as Fe and Cr is formed between 0 and 100 ps with an initial fast expansion, after 100 ps the expansion becomes slow, resulting in a corresponding initial signal enhancement and then a constant signal up to 350 ps, where the range of that experiment ended. Guo et al [41] studied the plasma expansion of fs-laser-induced plasma on GaP crystal for longer inner pulse delays and concluded that the electron density of the ejected plasma has a high value in the first 1.8 ns and then decreases. The above-mentioned results are in general agreement with our own observations on complex biological samples, albeit on a slightly different time scale.

Furthermore, all Ca lines exhibit a substantial increase at an inner pulse delay of 1100 ps, a feature which was reproducible across the measurements performed in the same conditions. We therefore consider this value of 1100 ps as appropriate for subsequent measurements.

3.2. Discrimination with ANN and RF algorithms

To determine the effect of double pulses on tissue discrimination by ML algorithms, spectra of liver and muscle tissue were recorded for SP and DP as before. The total energy used here was 7 μ J per pulse (14 μ J in the case of SP), which was slightly lower than in the previous experiment to avoid blasting the sample and recording spectra from the substrate. The discrimination of the two tissue types was tested for each algorithm (ANN and RF) and pulse case (SP and DP at 1100 ps). Following the removal of outliers and averaging, the number of remaining spectra for the algorithms to analyse is 506 for liver and 460 for muscle in the case

of SP and 482 for liver and 505 for muscle in the case of DP. The results from the algorithms are produced in the form of a confusion matrix, in which the predictions of the algorithms are displayed as true positives, true negatives, false positives and false negatives.

Fig. 4 shows the percentage of correct predictions (true positives) for each tissue type (liver and muscle) in both pulse cases (SP and DP) for both algorithms (ANN and RF). The data are presented in a scale beginning with 50 % correct prediction, which represents the point at which the algorithm predictions become random. Once the percentage of correct predictions exceeds 50 %, the performance of the algorithm is considered to be admissible.

The ANN algorithm can correctly predict the liver tissue in 73.7 % of the cases for the SP (light green bar) and 88.2 % in the case of DP (dark green). This represents a relative increase in accuracy by 19 % from SP to DP. For muscle tissue, the ANN presents more difficulties with correctly identifying the tissue; however, it does exhibit a 36 % increase of correct predictions from SP (64.8 %; light orange) to DP (88.7 %, dark orange).

In comparison to ANN, RF shows a considerably lower increase in correctly identifying the liver tissue (9 %). Both SP and DP demonstrated comparable accuracy in identifying the tissue (76.1 % and 83.2 %, respectively; blue bars). In the case of the SP on muscle, RF was unable to distinguish between muscle and liver tissue, and therefore attributed the tissue nearly randomly, with only 54.6 % correct predictions (light red). Regarding the DP on muscle, the results demonstrate that the RF algorithm is capable of correctly identifying the tissue in 85.5 % of instances (dark red), representing the greatest increase observed between SP and DP, with a 56 % improvement. A potential explanation for the observed disparities in the enhancements of the two tissue types may be attributed to their distinct morphological characteristics, although further research is needed.

In general, the utilization of double pulse instead of single pulse leads to more accurate predictions, regardless of the used algorithm. One potential explanation for the observed improvement in discrimination is the enhancement in signal-to-noise ratio. For this analysis, the full spectrum was processed in Orange with the widget 'SNR', which generates a numerical value for each pixel in the data set. SNR is the ratio of the mean signal of one wavelength within the spectrum and the standard deviation of the noise of this wavelength among hundreds of recorded spectra. The numerical values of SNR at the region where the most prominent lines are (C—N band (the highest one), Ca I and Na I lines)

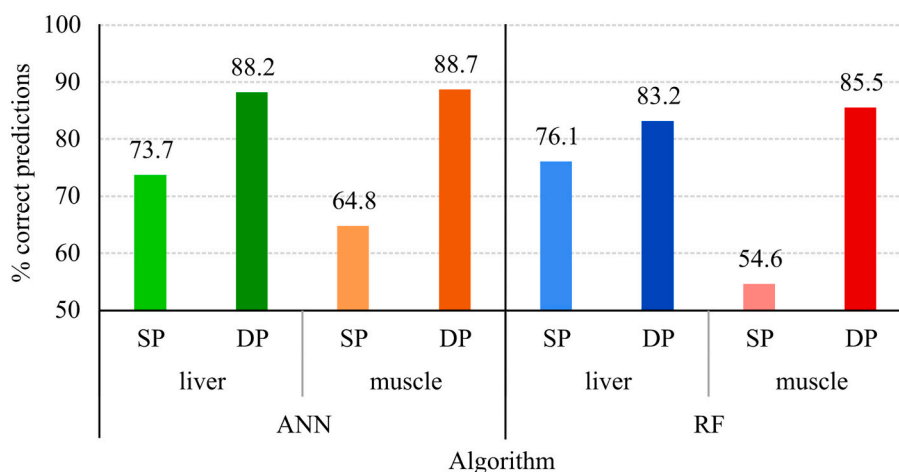


Fig. 4. Percentage of correct predictions from ANN and RF algorithms for liver (green and blue) and muscle tissue (orange and red), each in case of SP (lighter colors) and DP measurements (darker colors), respectively. (For interpretation of the references to color in this figure legend, the reader is referred to the web version of this article.)

were averaged and the results are presented in Table 1.

The greatest increase in SNR between SP and DP is observed in liver tissue for the C–N band with an improvement of up to 44 % (from 1.75 for the SP to 2.52 for DP). A comparable outcome is observed for the Na I line, with an improvement in SNR of 40 %. In the case of the Ca I line, the improvements are less pronounced (from 1.22 to 1.43). However, as indicated in the Introduction section, the molecular lines are more effectively displayed by fs-LIBS, while the atomic lines are more effectively displayed by ns-LIBS [9].

In conclusion, our results indicate that DP-LIBS offers a superior signal compared to SP-LIBS, a better SNR and therefore broader access to spectral lines.

4. Conclusions

In this paper, the discrimination of two tissue types by LIBS and machine learning algorithms has been successfully enhanced by implementing a double-pulse configuration. We demonstrate that double-pulse LIBS is a superior technique compared with single-pulse LIBS, offering better signal intensity and signal-to-noise ratio. The inner pulse delay of DP-LIBS was optimized on thin samples of liver tissue, and the results revealed that at 1100 ps inner delay between two consecutive pulses, the signal was the highest overall for all identified lines, with up to a fivefold increase. Furthermore, it was possible to access additional spectral information while maintaining the same total pulse energy.

Additionally, the implemented models of machine learning correctly predicted the tissue type with a higher percentage for the double-pulse configuration than using single-pulse. The enhancement factor varied between the tissue type and the model used, but overall, the liver tissue had a lower enhancement factor (19 % for ANN and 9 % for RF) compared to muscle tissue (36 % for ANN and 56 % for RF). Nevertheless, accessing superior signals through DP-LIBS and a higher signal-to-noise ratio resulted in enhanced discrimination for the most prominent lines. In the following years, the superior ablation quality of femtosecond lasers has the potential to become a key tool for biological tissue analysis, enabling micrometer-scale resolution and high accuracy elemental mapping [17,26]. The integration of fs-DP-LIBS with ML algorithms opens the door for the advancement of *in situ/in vivo* cancer detection, with the potential to achieve an enhanced signal-to-noise ratio and improved accuracy in the identification of tumor and non-tumor tissue.

Table 1

Average SNR for the spectral region of the C–N band, and Ca I and Na I lines for liver and muscle tissue.

Tissue	Line	SP	DP	%increase
Liver	C–N	1.75	2.52	44
	Ca I	1.22	1.43	17
	Na I	3.06	4.30	40
	C–N	1.82	2.46	35
Muscle	Ca I	1.25	1.53	22
	Na I	2.91	3.62	24

Declaration of generative AI and AI-assisted technologies in the writing process

During the preparation of this work, the author Elena Ramela Ciobotea used the online-free version of DeepL write tool to improve the readability and language of the manuscript. After using this tool, the author reviewed and edited the content as needed and takes full responsibility for the content of the published article.

CRedit authorship contribution statement

Elena Ramela Ciobotea: Writing – review & editing, Writing – original draft, Methodology, Investigation, Formal analysis, Data curation, Conceptualization. **Cristian Sarpe:** Writing – review & editing, Methodology, Investigation, Conceptualization. **Bastian Zielinski:** Writing – review & editing, Software, Methodology, Formal analysis, Conceptualization. **Hendrike Braun:** Writing – review & editing. **Arne Senftleben:** Writing – review & editing. **Soumi Dutta:** Writing – review & editing, Resources. **Georg Mayer:** Writing – review & editing, Resources. **Camilo Florian:** Writing – review & editing, Supervision. **Thomas Baumert:** Writing – review & editing, Supervision, Funding acquisition.

Declaration of competing interest

The authors declare that they have no known competing financial interests or personal relationships that could have appeared to influence the work reported in this paper.

Acknowledgments

This work was embedded in the project BiTWerk funded by the

University of Kassel.

Data availability

Data will be made available on request.

References

- W. Wessel, A. Brueckner-Foitz, J. Mildner, L. Englert, L. Haag, A. Horn, M. Wollenhaupt, T. Baumert, Use of femtosecond laser-induced breakdown spectroscopy (fs-LIBS) for micro-crack analysis on the surface, *Eng. Fract. Mech.* 77 (2010) 1874–1883, <https://doi.org/10.1016/j.engfracmech.2010.03.020>.
- L. Sun, H. Yu, Z. Cong, H. Lu, B. Cao, P. Zeng, W. Dong, Y. Li, Applications of laser-induced breakdown spectroscopy in the aluminum electrolysis industry, *Spectrochimica Acta Part B: Atomic Spectroscopy* 142 (2018) 29–36, <https://doi.org/10.1016/j.sab.2018.02.005>.
- A. Doña-Fernández, I. de Andres-Gimeno, P. Santiago-Toribio, E. Valtuille-Fernández, F. Aller-Sanchez, A. Heras-González, Real-time detection of GSR particles from crime scene: a comparative study of SEM/EDX and portable LIBS system, *Forensic Sci. Int.* 292 (2018) 167–175, <https://doi.org/10.1016/j.forsciint.2018.09.021>.
- M. Markiewicz-Keszycza, X. Cama-Moncunill, M.P. Casado-Gavalda, Y. Dixit, R. Cama-Moncunill, P.J. Cullen, C. Sullivan, Laser-induced breakdown spectroscopy (LIBS) for food analysis: a review, *Trends Food Sci. Technol.* 65 (2017) 80–93, <https://doi.org/10.1016/j.tifs.2017.05.005>.
- J. Wang, L. Li, P. Yang, Y. Chen, Y. Zhu, M. Tong, Z. Hao, X. Li, Identification of cervical cancer using laser-induced breakdown spectroscopy coupled with principal component analysis and support vector machine, *Lasers Med. Sci.* 33 (2018) 1381–1386, <https://doi.org/10.1007/s10103-018-2500-2>.
- B.S. Idrees, Q. Wang, M.N. Khan, G. Teng, X. Cui, W. Xiangli, K. Wei, In-vitro study on the identification of gastrointestinal stromal tumor tissues using laser-induced breakdown spectroscopy with chemometric methods, *Biomed. Opt. Express* 13 (2022) 26–38, <https://doi.org/10.1364/BOE.442489>.
- A. Assion, M. Wollenhaupt, L. Haag, F. Mayorov, C. Sarpe-Tudoran, M. Winter, U. Kutschera, T. Baumert, Femtosecond laser-induced breakdown spectrometry for Ca²⁺ analysis of biological samples with high spatial resolution, *Appl. Phys. B Lasers Opt.* 77 (2003) 391–397, <https://doi.org/10.1007/s00340-003-1262-z>.
- Y. Chen, J. Si, X. Wan, Y. Wang, A. Chen, M. Jin, Sub-ppb detection limit of Cr, Pb, and Cu in water by surface-enhanced LIBS with femtosecond laser, *Spectrochimica Acta Part B: Atomic Spectroscopy* 213 (2024) 106880, <https://doi.org/10.1016/j.sab.2024.106880>.
- S. Sunku, M.K. Gundawar, A.K. Myakalwar, P.P. Kiran, S.P. Tewari, S.V. Rao, Femtosecond and nanosecond laser induced breakdown spectroscopic studies of NTO, HMX, and RDX, *Spectrochimica Acta Part B: Atomic Spectroscopy* 79–80 (2013) 31–38, <https://doi.org/10.1016/j.sab.2012.11.002>.
- E.N. Rao, P. Mathi, S.A. Kalam, S. Sreedhar, A.K. Singh, B.N. Jagatap, S.V. Rao, Femtosecond and nanosecond LIBS studies of nitroimidazoles: correlation between molecular structure and LIBS data, *J. Anal. At. Spectrom* 31 (2016) 737–750, <https://doi.org/10.1039/C5JA00445D>.
- A. Elhassan, A. Giakoumaki, D. Anglos, G.M. Ingo, L. Robbiola, M.A. Harith, Nanosecond and femtosecond laser induced breakdown spectroscopic analysis of bronze alloys, *Spectrochimica Acta Part B: Atomic Spectroscopy* 63 (2008) 504–511, <https://doi.org/10.1016/j.sab.2008.02.003>.
- O.A. Nassef, H.E. Elsayed-Ali, Spark discharge assisted laser induced breakdown spectroscopy, *Spectrochimica Acta Part B: Atomic Spectroscopy* 60 (2005) 1564–1572, <https://doi.org/10.1016/j.sab.2005.10.010>.
- X. Zhang, X. Li, X. Chen, M. Shi, T. Ren, Nanoparticle-enhanced laser-induced breakdown spectroscopy for serum element analysis using an Ag NP-coated filter paper substrate, *J. Anal. At. Spectrom* 39 (2024) 1332–1342, <https://doi.org/10.1039/D3JA00462G>.
- V.H.C. Ferreira, V. Gardette, B. Busser, L. Sancey, S. Ronsmans, V. Bonnetterre, V. Motto-Ros, L. Duponchel, Enhancing diagnostic capabilities for occupational lung diseases using LIBS imaging on biopsy tissue, *Anal. Chem.* 96 (2024) 7038–7046, <https://doi.org/10.1021/acs.analchem.4c00237>.
- L. Yang, M. Liu, Y.-T. Liu, Q.-X. Li, S.-Y. Li, Y.-F. Jiang, A.-M. Chen, M.-X. Jin, Influence of polarization of laser beam on emission intensity of femtosecond laser-induced breakdown spectroscopy*, *Chinese Phys. B* 29 (2020) 65203, <https://doi.org/10.1088/1674-1056/ab84dc>.
- Q. Wang, A. Chen, W. Xu, S. Li, Y. Jiang, M. Jin, Signal improvement using circular polarization for focused femtosecond laser-induced breakdown spectroscopy, *J. Anal. At. Spectrom* 34 (2019) 1242–1246, <https://doi.org/10.1039/C9JA00033J>.
- J. Mildner, C. Sarpe, N. Götte, M. Wollenhaupt, T. Baumert, Emission signal enhancement of laser ablation of metals (aluminum and titanium) by time delayed femtosecond double pulses from femtoseconds to nanoseconds, *Appl. Surf. Sci.* 302 (2014) 291–298, <https://doi.org/10.1016/j.apsusc.2013.09.137>.
- J.P. McDonald, D.K. Das, J.A. Nees, T.M. Pollock, S.M. Yalisove, Approaching non-destructive surface chemical analysis of CMSX-4 superalloy with double-pulsed laser induced breakdown spectroscopy, *Spectrochimica Acta Part B: Atomic Spectroscopy* 63 (2008) 561–565, <https://doi.org/10.1016/j.sab.2008.02.004>.
- E.J. Kautz, M.P. Polek, E.C. Rönnebro, S.S. Harilal, Enhancing analytical merits of laser-induced breakdown spectroscopy of hydrogen isotopes using an orthogonal double-pulsing scheme, *Spectrochimica Acta Part B: Atomic Spectroscopy* 217 (2024) 106952, <https://doi.org/10.1016/j.sab.2024.106952>.
- Y. Lu, V. Zorba, X. Mao, R. Zheng, R.E. Russo, UV fs–ns double-pulse laser induced breakdown spectroscopy for high spatial resolution chemical analysis, *J. Anal. At. Spectrom* 28 (2013) 743, <https://doi.org/10.1039/c3ja30315b>.
- Y. Wang, A. Chen, Q. Wang, D. Zhang, S. Li, Y. Jiang, M. Jin, Study of signal enhancement in collinear femtosecond-nanosecond double-pulse laser-induced breakdown spectroscopy, *Opt. Laser Technol.* 122 (2020) 105887, <https://doi.org/10.1016/j.optlastec.2019.105887>.
- Y. Li, Y. Chen, Y. Jiang, Z. Wang, X. Huang, Detection of gold alloy elements by target-enhanced orthogonal triple-pulse laser-induced breakdown spectroscopy with improved sensitivity and minimal sample ablation, *Spectrochimica Acta Part B: Atomic Spectroscopy* 213 (2024) 106862, <https://doi.org/10.1016/j.sab.2024.106862>.
- D. Prochazka, P. Pořízka, J. Novotný, A. Hrdlička, K. Novotný, P. Šperka, J. Kaiser, Triple-pulse LIBS: laser-induced breakdown spectroscopy signal enhancement by combination of pre-ablation and re-heating laser pulses, *J. Anal. At. Spectrom* 35 (2020) 293–300, <https://doi.org/10.1039/C9JA00323A>.
- J. Scaffidi, J. Pender, W. Pearman, S.R. Goode, B.W. Colston, J.C. Carter, S. M. Angel, Dual-pulse laser-induced breakdown spectroscopy with combinations of femtosecond and nanosecond laser pulses, *Appl. Optics* 42 (2003) 6099–6106.
- A. El-Hussein, A.K. Kassem, H. Ismail, M.A. Harith, Exploiting LIBS as a spectrochemical analytical technique in diagnosis of some types of human malignancies, *Talanta* 82 (2010) 495–501, <https://doi.org/10.1016/j.talanta.2010.04.064>.
- B. Busser, S. Moncayo, F. Trichard, V. Bonnetterre, N. Pinel, F. Pelascini, P. Dugourd, J.-L. Coll, M. D'Incan, J. Charles, V. Motto-Ros, L. Sancey, Characterization of foreign materials in paraffin-embedded pathological specimens using in situ multi-elemental imaging with laser spectroscopy, *Mod. Pathol.* 31 (2018) 378–384, <https://doi.org/10.1038/modpathol.2017.152>.
- Y. Gimenez, B. Busser, F. Trichard, A. Kulesza, J.M. Laurent, V. Zaun, F. Lux, J. M. Benoit, G. Panczer, P. Dugourd, O. Tillement, F. Pelascini, L. Sancey, V. Motto-Ros, 3D imaging of nanoparticle distribution in biological tissue by laser-induced breakdown spectroscopy, *Sci. Rep.* 6 (2016) 29936, <https://doi.org/10.1038/srep29936>.
- L. Sancey, S. Kotb, C. Truillet, F. Appaix, A. Marais, E. Thomas, B. van der Sanden, J.-P. Klein, B. Laurent, M. Cottier, R. Antoine, P. Dugourd, G. Panczer, F. Lux, P. Perriat, V. Motto-Ros, O. Tillement, Long-term in vivo clearance of gadolinium-based AgAuX nanoparticles and their biocompatibility after systemic injection, *ACS Nano* 9 (2015) 2477–2488, <https://doi.org/10.1021/acsnano.5b00552>.
- F.-Y. Yueh, H. Zheng, J.P. Singh, S. Burgess, Preliminary evaluation of laser-induced breakdown spectroscopy for tissue classification, *Spectrochim. Acta B At. Spectrosc.* 64 (2009) 1059–1067, <https://doi.org/10.1016/j.sab.2009.07.025>.
- E.J. Blanchette, E.A. Tracey, A. Baughan, G.E. Johnson, H. Malik, C.N. Alionte, I. G. Arthur, M. Pontoni, S.J. Rehe, Detection and diagnosis of bacterial pathogens in urine using laser-induced breakdown spectroscopy, *Spectrochimica Acta Part B: Atomic Spectroscopy* 216 (2024) 106944, <https://doi.org/10.1016/j.sab.2024.106944>.
- A. Kumar, F.Y. Yueh, J.P. Singh, S. Burgess, Characterization of malignant tissue cells by laser-induced breakdown spectroscopy, *Appl. Optics* 43 (2004) 5399.
- S. Moncayo, L. Duponchel, N. Mousavipak, G. Panczer, F. Trichard, B. Bousquet, F. Pelascini, V. Motto-Ros, Exploration of megapixel hyperspectral LIBS images using principal component analysis, *J. Anal. At. Spectrom* 33 (2018) 210–220, <https://doi.org/10.1039/C7JA00398F>.
- A. Nardecchia, C. Fabre, J. Cauzid, F. Pelascini, V. Motto-Ros, L. Duponchel, Detection of minor mineral compounds in complex mineral samples from millions of spectra: a new data analysis strategy in LIBS imaging, *Anal. Chim. Acta* 1114 (2020) 66–73, <https://doi.org/10.1016/j.aca.2020.04.005>.
- Y. Chu, T. Chen, F. Chen, Y. Tang, S. Tang, H. Jin, L. Guo, Y.F. Lu, X. Zeng, Discrimination of nasopharyngeal carcinoma serum using laser-induced breakdown spectroscopy combined with an extreme learning machine and random forest method, *J. Anal. At. Spectrom* 33 (2018) 2083–2088, <https://doi.org/10.1039/C8JA00263K>.
- C. Sarpe, E.R. Ciobotea, C.B. Morscher, B. Zieliński, H. Braun, A. Senftleben, J. Rüschoff, T. Baumert, Identification of tumor tissue in thin pathological samples via femtosecond laser-induced breakdown spectroscopy and machine learning, *Sci. Rep.* 13 (2023) 9250, <https://doi.org/10.1038/s41598-023-36155-8>.
- G. Chen, G. Yang, Z. Ling, Y. Yang, Y. Zhan, X. Jin, The parameter optimization of lasers' energy ratio of the double-pulse laser induced breakdown spectrometry for heavy metal elements in the soil, *Anal. Methods* 13 (2021) 1502–1510, <https://doi.org/10.1039/d1ay00237f>.
- Janez Demšar, Tomaž Curk, Aleš Erjavec, Črt Gorup, Tomaž Hočevar, Mitar Milutinović, Martin Možina, Matija Poljanec, Marko Toplak, Anže Starič, Miha Štajdohar, Lan Umek, Lan Zagar, Jure Zbonjar, Marinka Žitnik, Blaž Zupan, Orange: data mining toolbox in Python, *J. Mach. Learn. Res. (Journal of Machine Learning Research)* 14 (2013) 2349–2353.
- A. Kramida, Y. Ralchenko, NIST Atomic Spectra Database, NIST Standard Reference Database 78, National Institute of Standards and Technology, 1999.
- J. Moros, J. Laserna, Laser-induced breakdown spectroscopy (LIBS) of organic compounds: a review, *Appl. Spectrosc.* 73 (2019) 963–1011, <https://doi.org/10.1177/0003702819853252>.
- Y. Wang, A. Chen, S. Li, L. Sui, D. Liu, D. Tian, Y. Jiang, M. Jin, Enhancement of laser-induced Fe plasma spectroscopy with dual-wavelength femtosecond double-pulse, *J. Anal. At. Spectrom* 31 (2016) 497–505, <https://doi.org/10.1039/C5JA00420A>.
- J. Guo, M. Wang, Q. Guo, T. Zhu, M. Du, P. Zhao, L. Feng, Lifetime visualization of femtosecond laser-induced plasma on GaP crystal, *Opt. Express* 31 (2023) 6877–6889, <https://doi.org/10.1364/OE.480338>.